analytical chemistry

Article

pubs.acs.org/ac

Sensitive Targeted Quantification of ERK Phosphorylation Dynamics and Stoichiometry in Human Cells without Affinity Enrichment

Tujin Shi,[†] Yuqian Gao,[†] Matthew J. Gaffrey,[†] Carrie D. Nicora,[†] Thomas L. Fillmore,[‡] William B. Chrisler,[†] Marina A. Gritsenko,[†] Chaochao Wu,[†] Jintang He,[†] Kent J. Bloodsworth,[†] Rui Zhao,[‡] David G. Camp, II,[†] Tao Liu,[†] Karin D. Rodland,[†] Richard D. Smith,[†] H. Steven Wiley,*[,‡] and Wei-Jun Qian*[,†]

[†]Biological Sciences Division, Pacific Northwest National Laboratory, Richland, Washington 99354, United States

[‡]Environmental Molecular Sciences Laboratory, Pacific Northwest National Laboratory, Richland, Washington 99354, United States

Supporting Information

ABSTRACT: Targeted mass spectrometry is a promising technology for site-specific quantification of posttranslational modifications. However, a major constraint is the limited sensitivity for quantifying low-abundance PTMs, requiring the use of affinity reagents for enrichment. Herein, we demonstrate the direct site-specific quantification of ERK phosphorylation isoforms (pT, pY, pTpY) and their relative stoichiometry using a sensitive targeted MS approach termed high-pressure, high-resolution separations with intelligent selection, and multiplexing (PRISM). PRISM provides effective enrichment of target peptides into a given fraction from complex mixture, followed by selected reaction monitoring quantification. Direct quantification of ERK phosphorylation in human mammary epithelial cells (HMEC) was demonstrated from as little as 25 μg tryptic peptides from whole cell lysates. Compared to immobilized metal-ion affinity chromatography, PRISM provided ~10-fold higher signal intensities, presumably due to the better peptide recovery of PRISM. This approach was applied to quantify ERK phosphorylation dynamics in HMEC treated by different doses of epidermal growth factor at both the peak activation (10 min) and steady state (2 h). The maximal ERK activation was observed with 0.3 and 3 ng/mL doses for 10 min and 2 h time points, respectively. The dose−response profiles of individual phosphorylated isoforms showed that singly phosphorylated pT-ERK never increases significantly, while the increase of pY-ERK paralleled that of pTpY-ERK. This data supports for a processive, rather than distributed model of ERK phosphorylation. The PRISM-SRM quantification of protein phosphorylation illustrates the potential for simultaneous quantification of multiple PTMs.

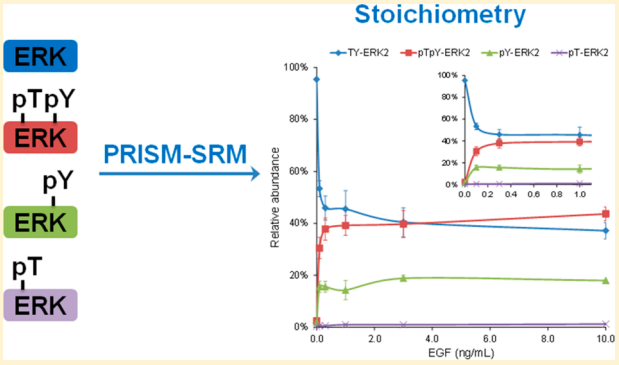

Signal transduction is often regulated by the reversible phosphorylation of proteins on serine, threonine, and tyrosine residues.[1,2] Traditional approaches for studying phosphorylation rely on site-specific antibodies for use in Western blots, ELISAs, flow cytometry, and protein arrays.[3,4] These approaches provide excellent quantitative information on protein phosphorylation; however, high-quality antibodies are generally not available for specific sites.[3] Selected reaction monitoring (SRM), also known as multiple reaction monitoring (MRM), is a promising technology for site-specific quantification of phosphorylation because of its high specificity, relatively good sensitivity and reproducibility.[5,6] Nevertheless, current SRM technologies still do not offer sufficient sensitivity for quantification of low-abundance phosphopeptides and affinity enrichment strategies are required prior to SRM detection.[3,5,7,8] Phosphorylated peptides are commonly enriched by ionic interaction-based affinity methods, such as immobilized metal affinity chromatography (IMAC) or titanium oxide (TiO_2); however, these methods have varying degrees of specificity and display bias for distinct sets of phosphorylated peptides.[2,9−13] For example, IMAC has a stronger affinity for multiply phosphorylated peptides than TiO_2, whereas TiO_2 tends to enrich singly phosphorylated peptides.[10,11,14] Moreover, these methods suffer significant sample loss and typically require relatively large amounts of starting materials for analysis (≥1 mg of whole cell lysate).[10−12]

Recently, we developed an affinity reagent-free strategy, termed high-pressure, high-resolution separation with intelligent selection and multiplexing (PRISM),[15−18] for selective enrichment of target peptides from a complex peptide mixture through high-resolution reversed phase liquid chromatography (LC) separation/fractionation. Application of this strategy to human blood plasma demonstrated a nearly 200-fold enhancement in SRM sensitivity for most target peptides, a level comparable to

Received: October 2, 2014
Accepted: December 17, 2014
Published: December 17, 2014

DOI: 10.1021/ac503797x
Anal. Chem. 2015, 87, 1103−1110

Table 1. Surrogate Peptides for ERK1/2 Isoforms and Three Best Transitions Selected for Each Target Peptide[a]

isoform	standard sequence	SRM transitions Q1	SRM transitions Q2
ERK1	LADPEHDHTGFLTEYVATR (TY-ERK1)	724.7	839.4 ($y7^+$), 738.4 ($y6^+$), 609.3 ($y5^+$)
	LADPEHDHTGFLpTEYVATR (pT-ERK1)	751.3	718.7 ($[precursor-98]^{3+}$), 821.4 ($[y7-98]^+$), 927.9 ($[y16-98]^{2+}$)
	LADPEHDHTGFLTEpYVATR (pY-ERK1)	751.3	919.4 ($y7^+$), 689.3 ($y5^+$), 976.9 ($y16^{2+}$)
	LADPEHDHTGFLpTEpYVATR (pTpY-ERK1)	778.0	745.3 ($[precursor-98]^{3+}$), 901.4 ($[y7-98]^+$), 967.9 ($[y16-98]^{2+}$)
ERK2	VADPDHDHTGFLTEYVATR (TY-ERK2)	715.3	952.5 ($y8^+$), 839.4 ($y7^+$), 738.4 ($y6^+$)
	VADPDHDHTGFLpTEYVATR (pT-ERK2)	742.0	709.3 ($[precursor-98]^{3+}$), 934.5 ($[y8-98]^+$), 738.4 ($y6^+$)
	VADPDHDHTGFLTEpYVATR (pY-ERK2)	742.0	919.4 ($y7^+$), 818.3 ($y6^+$), 689.3 ($y5^+$)
	VADPDHDHTGFLpTEpYVATR (pTpY-ERK2)	768.7	736.0 ($[precursor-98]^{3+}$), 901.4 ($[y7-98]^+$), 446.3 ($y4^+$)

[a]Masses listed are for the nature forms and stable isotopes (^{13}C and ^{15}N) were labeled on the C-terminal arginine residue.

immunoassays.[15−17] This level of sensitivity provides the potential for direct detection of low-abundance phosphorylated peptides or other PTMs in complex samples without affinity enrichment.

To demonstrate the direct targeted quantification of phosphorylation by PRISM, we utilized the extracellular signal-regulated kinase (ERK) as a model system and provided quantification of three distinct phosphoforms for both ERK1 and ERK2 in response to varying doses of epidermal growth factor (EGF) at multiple time points. As a paradigmatic signaling protein, ERK phosphorylation is often used for evaluation of analytical platforms because it has moderate complexity (i.e., two highly related isoforms, ERK1 and ERK2, phosphorylated on T and Y residues in a TEY motif within its activation loop),[4,19−22] and has been well studied in vitro and in vivo.[23−30] In this study, we demonstrate that PRISM-SRM provides a greater sensitivity for quantifying ERK phosphorylation compared to IMAC-SRM. Moreover, the sensitivity of PRISM-SRM was sufficient to enable quantification of all phosphorylated ERK isoforms at both basal and stimulated conditions, providing accurate estimates of phosphorylation stoichiometries and their dose responses in a well-studied model system.

EXPERIMENTAL SECTION

Reagents. Urea, dithiothreitol (DTT), iodoacetamide, ammonium formate, acetic acid, trifluoroacetic acid (TFA), and formic acid were obtained from Sigma (St. Louis, MO). Synthetic heavy peptides labeled with $^{13}C/^{15}N$ on the C-terminal arginine with >95% purity were purchased from Thermo Fisher Scientific (Rockford, IL). The magnetic Ni-NTA agarose beads were obtained from Qiagen (Valencia, CA).

ERK Surrogate Peptides. Eight tryptic peptides (i.e., 2 nonphosphorylated peptides and 6 phosphorylated peptides) were chosen based upon existing LC-MS/MS data. The eight peptides selected with their abbreviations are listed in Table 1. For each peptide, 3 transitions were selected and the best transition (i.e., the one with the most intense SRM signal and without evidence of coeluting interference) was used to quantify ERK phosphorylation and to determine their stoichiometries. The potential interference for given transitions were assessed based on the relative intensity ratios between the 3 transitions as previously reported.[15,17,18] Optimal collision energy values were achieved by direct infusion of each individual peptide.

Cell Culture, Treatment, and Protein Digestion. HMEC 184A1 was obtained from Martha Stampfer (Lawrence Berkeley National Laboratory)[26] and cultured and maintained in 75 cm^2 flasks in mammary epithelial cell basal medium (MEBM) supplemented with bovine pituitary extract (BPE), hydrocortisone, insulin, EGF (Fisher Scientific, Pittsburgh, PA), and 1% fetal bovine serum (Invitrogen, Carlsbad, CA). Cells were cultured at 37 °C with 5% CO_2 and 95% relative humidity. Prior to stimulation, cells were seeded into 100 mm culture plates, grown until near confluence and depleted of EGF by overnight culture in MEBM without EGF. For initial assessment of sensitivity, HMEC cells were treated with 10 ng/mL of EGF for 10 min. For dose−response experiments, EGF was added directly to culture plates to achieve the required dose (0, 0.1, 0.3, 1.0, 3.0, 10.0 ng/mL) for either 10 min or 2 h. After stimulation, cells (∼1 million per plate) were rinsed twice with ice cold PBS and harvested in 1 mL ice cold PBS containing 1% phosphatase inhibitor cocktail (Pierce, Rockford, IL) and 10 mM NaF (Sigma-Aldrich, St. Louis, MO). Cells were centrifuged at 1500 rpm for 10 min at 4 °C and excess PBS was carefully aspirated from cell pellet.

Cell pellets were resuspended in ice-cold cell lysis buffer (50 mM HEPES, 150 mM NaCl, 5 mM EDTA, 1% Triton X-100, pH 7.7). Cell lysates were centrifuged at 14 000 rpm at 4 °C for 10 min and soluble protein fraction was retained. Protein concentrations were determined by the BCA assay (Pierce, Rockford, IL); ∼200 μg proteins from each plate were denatured and reduced by 8 M urea and 10 mM DTT in 50 mM NH_4HCO_3 at pH 8.0 for 1 h at 37 °C. Protein cysteine residues were alkylated with 40 mM iodoacetamide for 1 h at room temperature. The resulting sample was diluted 6-fold with 50 mM NH_4HCO_3, pH 8.0, and digested by sequencing-grade modified porcine trypsin (Promega, Madison, WI) with a 1:50 trypsin/protein ratio (w/w) at 37 °C for overnight. The resulting digest was then desalted by using a 1 mL SPE C18 column (Supelco, Bellefonte, PA); ∼100 μg of peptides was obtained from each sample and the peptide sample was diluted to 0.5 μg/μL with 0.1% formic acid in water, and heavy isotope-labeled synthetic peptides at an equimolar concentration (5 fmol/μL or 20 fmol/μL) were spiked into the peptide mixture samples.

IMAC Enrichment. Approximately 25 μg of peptides from HMEC stimulated by 10 ng/mL EGF for 10 min or without stimulation were spiked with 20 fmol/μL of heavy labeled peptides and then subjected to IMAC for phosphopeptide enrichment. The magnetic Fe^{3+}-NTA agarose beads were prepared by replacing the Ni^{2+} ion on the magnetic Ni-NTA agarose beads (Qiagen, Valencia, CA) with Fe^{3+} through buffer exchange.[31] Peptides were reconstituted in 50 μL IMAC binding/wash buffer containing 80% ACN and 0.1% TFA and incubated for 30 min with 20 μL of the 5% preconditioned bead suspension. After incubation, the beads were washed 4 times with 50 μL of wash buffer. Phosphorylated peptides were eluted from the beads with elution buffer containing 50% acetonitrile and 5% ammonia in 5 mM phosphate buffer (pH 8). The eluate was acidified with acetic acid to a pH of ∼3.5 and concentrated to

DOI: 10.1021/ac503797x
Anal. Chem. 2015, 87, 1103−1110

~20 μL by vacuum centrifugation. Four μL of IMAC enriched samples was loaded onto the analytical column for LC-SRM analysis. The on-column peptide loading amounts were nearly equal to those in the later PRISM-SRM analysis to enable comparison of sensitivity and recovery.

PRISM Fractionation. The high pH reversed phase LC fractionation is one of the main components of the PRISM workflow (Supporting Information Figure S1), which was performed as previously described.[15,17]

LC-SRM Analysis. Following the intelligent selection (*iSelection*) of target peptide fractions, the peptide fraction of interest was subjected to LC-SRM measurement (Supporting Information Figure S1). All peptide fractions were analyzed using the nanoACQUITY UPLC system coupled online to a TSQ Vantage triple quadrupole mass spectrometer (Thermo Scientific, San Jose, CA). Solvents used were 0.1% formic acid in water (mobile phase A) and 0.1% formic acid in 90% acetonitrile (mobile phase B). Peptide fraction samples were loaded onto a 5 μm C18 trap column (180 μm i.d. × 20 mm) for 5 min at 10 μL/min with 3% B. Peptide separations were performed at a flow rate of 400 nL/min using a BEH 1.7 μm C18 column (100 μm i.d. × 10 cm), which was connected to a chemically etched 20 μm i.d. fused-silica emitter via a conductive carbon fiber peek union (for avoiding phosphorylated peptide loss during electrospray ionization). Either 1 μL of unfractionated digest or 4 μL of individual fractions (total volume 20 μL; ~50 ng was loaded onto the analytical column for LC-SRM analysis) following PRISM was injected for LC separations using a binary gradient of 10−20% B in 7 min, 20−25% B in 17 min, 25−40% B in 1.5 min, 40−95% B in 2.5 min and at 95% B for 6 min for a total of ~35 min and the analytical column was re-equilibrated at 98% A for 15 min. A dwell time of 40 ms was used for all SRM transitions.

Data Analysis. SRM data were analyzed using Skyline software.[32] The relative signal intensities of the 3 selected transitions for each peptide were predefined by internal standard heavy peptides spiked into the buffer. Matrix inferences from coeluting peptides with a transition that falls within the mass width of Q1 and Q3 were detected by deviation from the expected signal ratios between the transitions. The best transition for each peptide was used for quantification. Peak detection and integration were determined based on two criteria: (1) same retention time and (2) approximately the same relative SRM peak intensity ratios across multiple transitions between light peptides and heavy peptide standards. Standard derivation (SD) and coefficient of variation (CV) were calculated based on three biological replicates of measurements at each EGF dose point or time-course point. All data were manually inspected to ensure correct peak detection and accurate integration. Signal to noise ratio (S/N) was calculated by the peak apex intensity over the highest background noise in a retention time region of ±15 s for the target peptides. The background noise levels were conservatively estimated by visually inspecting chromatographic peak regions. A S/N of surrogate endogenous phosphopeptides >10 is required for confident quantification.

RESULTS

Proof-of-Concept. To determine whether direct PRISM-SRM (i.e., without affinity enrichment) had sufficient sensitivity for quantifying phosphopeptides, PRISM-SRM was compared to conventional LC-SRM for targeted quantification of endogenous ERK phosphorylation in the HMEC at the peak activation state (i.e., treated with 10 ng/mL EGF for 10 min) using the target peptides covering Ser 198 and Thr 202 (Table 1). Although LC-SRM could detect nonphosphorylated ERK peptides, none of the phosphorylated ERK peptides were detected (Supporting Information Figure S2). By contrast, PRISM-SRM readily detected both phosphorylated and nonphosphorylated peptides (Figure 1A) with all three ERK2 phosphorylated peptides being quantifiable. PRISM-SRM also enabled detection and quantification of all three ERK1 phosphorylated peptides but with lower abundance compared to ERK2 phosphorylation (Supporting Information Figure S2A). Note that all isotope-labeled ERK1 synthetic peptides have slightly later retention times than their corresponding endogenous peptides, which are presumably because of different conformations between the synthetic internal standards and their native endogenous peptides for proline-containing peptides (Supporting Information Figure S2A). Importantly, the relative abundance patterns between different transitions were the same for both endogenous and synthetic peptides when both versions of peptides were confidently detected.

Figure 1B further illustrated that PRISM-SRM provided sufficient sensitivity for reproducible quantification of mono-phosphorylated pY-ERK2 and dual-phosphorylated pTpY-ERK2 in HMEC even at basal conditions. But the monophosphorylated pT-ERK2 was not confidently detected due to its low-abundance. This result is consistent with but more informative than Western blotting analysis in quantitative measurements of ERK2 phosphorylation[19,26,33] because PRISM-SRM can provide accurate molar abundance and stoichiometry of individual ERK2 phosphorylated isoforms. Unfortunately, none of the low abundance ERK1 phosphorylated peptides was confidently detected under the basal condition (Supporting Information Figure S2B). Based on the ratio of endogenous light over the heavy peptide peak area (i.e., L/H ratio) in the unstimulated HMEC cells and the known concentration of the spiked-in heavy internal standard, the concentrations of the non-, mono-, and dual-phosphorylated ERK2 forms at the basal and following 10 min stimulation with 10 ng/mL of EGF were estimated as molecules per cell (i.e., protein copy number per cell) (Figure 1C). The sensitivity of PRISM-SRM for quantification of ERK phosphorylation was assessed based on the estimated molar abundance pT-ERK2 when a S/N was ~10. Under the basal conditions the abundance of pT-ERK2 was calculated to be ~700 molecules per cell (corresponding to 0.4% of the total ERK2 levels) with a S/N of 5; whereas at 10 ng/mL of EGF stimulation conditions the calculated abundance of pT-ERK2 was ~1900 molecules per cell (corresponding to 1.2% of the total ERK2 levels) with a S/N of 17 (Figure 1C and Supporting Information Methods). Therefore, PRISM-SRM provides a level of sensitivity of ~1000 molecules per cell in quantifying ERK phosphorylation.

PRISM-SRM versus IMAC-SRM. Next, we performed a side-by-side comparison of PRISM-SRM with IMAC-SRM; ~50 μg of tryptic digest from cells treated with 10 ng/mL of EGF for 10 min was divided into two aliquots with ~25 μg each: one for PRISM, the other for IMAC. All the endogenous ERK phosphorylated peptides were reproducibly detected by PRISM-SRM; whereas only the most abundant dual-phosphorylated peptides, pTpY-ERK1 and pTpY-ERK2, were reliably detected by IMAC-SRM (Figure 2 and Supporting Information Figure S3). To determine the reproducibility of IMAC enrichment for the relatively small-size samples, two processing replicates were analyzed. The similar levels of SRM signals (i.e., peak intensity) of heavy internal standards between the two

DOI: 10.1021/ac503797x
Anal. Chem. 2015, 87, 1103−1110

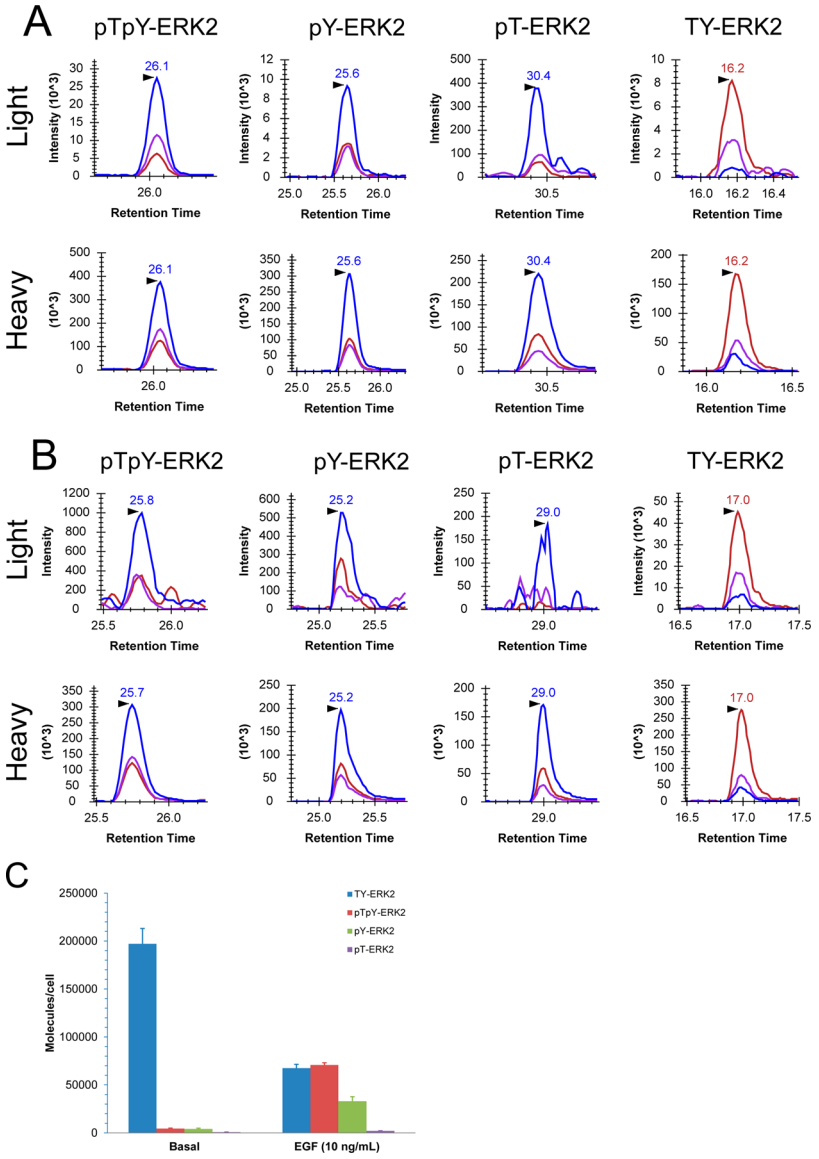

Figure 1. PRISM-SRM detection of ERK phosphorylation in the HMEC. (A) XICs of transitions monitored for ERK2 phosphorylation treated with 10 ng/mL EGF for 10 min. (B) XICs of transitions monitored for ERK2 phosphorylation without stimulation. pTpY-ERK2:768.7/736.0 (blue), 768.7/901.4 (purple), 768.7/446.3 (brown); pY-ERK2:742.0/919.4 (blue), 742.0/818.3 (purple), 742.0/689.3 (brown); pT-ERK2:742.0/709.3 (blue), 742.0/934.5 (purple), 742.0/738.4 (brown); TY-ERK2:715.3/839.4 (brown), 715.3/748.4 (purple), 715.3/962.5 (blue). (C) Molar abundances of the non-, mono-, and double-phosphorylated ERK2 isoforms with standard derivation (n = 3) at the basal and 10 ng/mL EGF levels after 10 min stimulation.

replicates illustrate the reproducibility of IMAC enrichment (Supporting Information Table S1). By comparing the SRM signals from IMAC-SRM with PRISM-SRM, the recovery of phosphorylated peptides from IMAC enrichment was estimated to be only 4−10% of that from PRISM based on data from two replicates, suggesting that the high pH reversed-phase LC in the PRISM workflow offers significantly higher recovery for phosphopeptides than IMAC for handling relatively small samples (Supporting Information Table S1). The low recovery of IMAC may be in part due to the low amount of starting material (~25 μg), which could lead to a significant degree of nonspecific loss during sample handling. Furthermore, we noted that the dual-phosphorylated peptides had slightly higher recovery following IMAC enrichment when compared to the monophosphorylated peptides, that is, 10.6% for pTpY-ERK, 8.0% for pY-ERK, and 4.0% for pT-ERK, which is consistent with previous reports that IMAC favors the selective enrichment of multiphosphorylated peptides and has a negative bias for monophosphorylated peptides.[10,11,14]

Quantification of ERK Phosphorylation Dynamics in EGF-Induced Dose Responses. PRISM-SRM was applied to measure the dynamics of ERK phosphorylation in HMEC exposed to low to medium doses of EGF. Cells were stimulated for either 10 min (to measure peak activation) or 2 h (to measure steady state levels of phosphorylation) with EGF concentrations ranging from 0.1 to 10 ng/mL. The quantified levels of ERK phosphorylation were used to calculate the relative stoichiometry for each ERK isoform (e.g., unphosphorylated TY-ERK, singly phosphorylated pT-ERK and pY-ERK, and doubly phosphorylated pTpY-ERK) in percentage of total abundance of ERK. The percentage was calculated based on the L/H area ratio of each individual isoform divided by the total L/H area ratio of all ERK

DOI: 10.1021/ac503797x
Anal. Chem. 2015, 87, 1103−1110

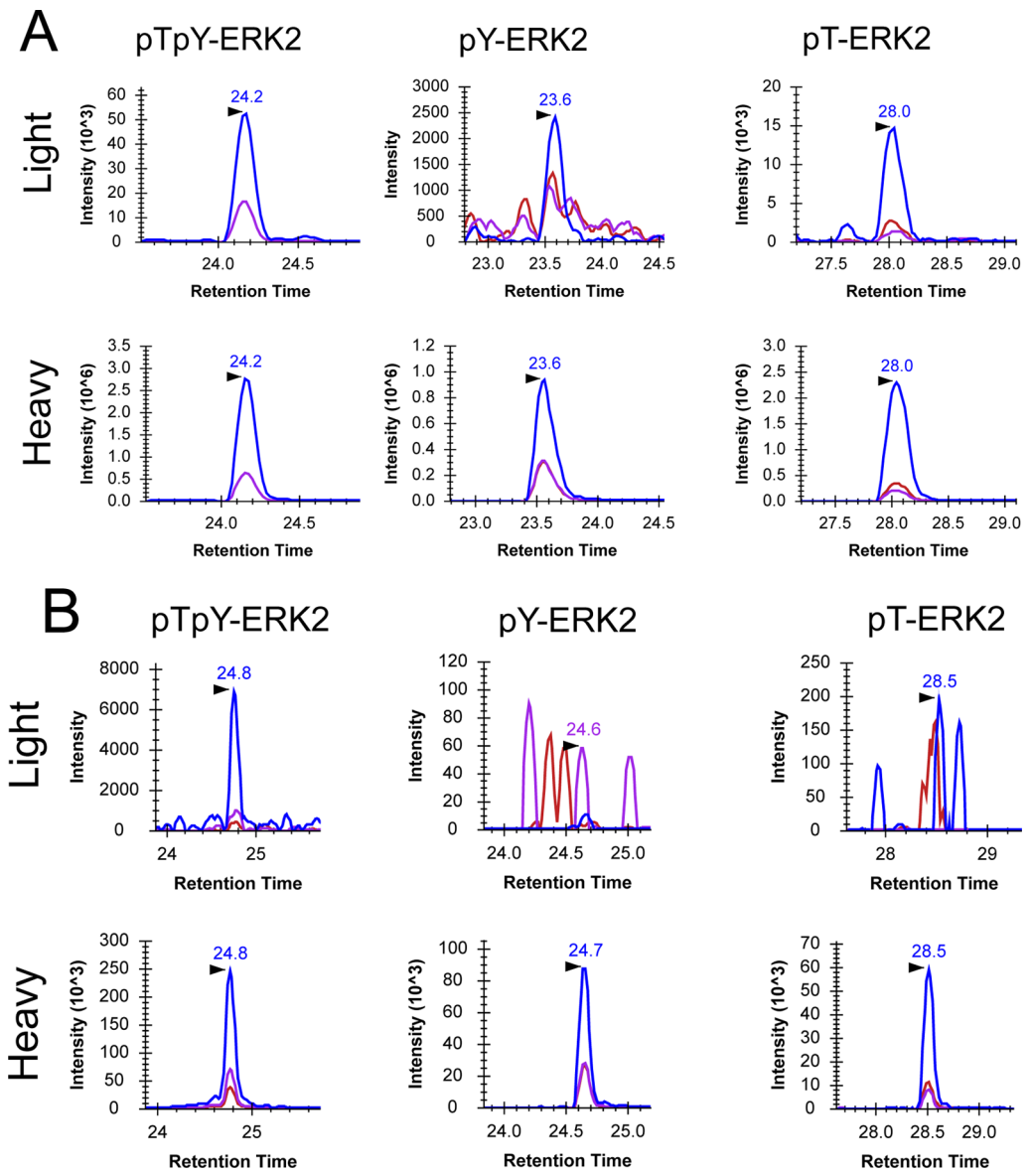

Figure 2. PRISM-SRM vs IMAC-SRM for quantification of ERK2 phosphorylation in HMEC stimulated by 10 ng/mL EGF for 10 min in an independent batch of cell culture. (A) PRISM-SRM. (B) IMAC-SRM. pTpY-ERK2:768.7/736.0 (blue), 768.7/901.4 (purple), 768.7/446.3 (brown); pY-ERK2:742.0/919.4 (blue), 742.0/818.3 (purple), 742.0/689.3 (brown); pT-ERK2:742.0/709.3 (blue), 742.0/934.5 (purple), 742.0/738.4 (brown). Equal amounts of HMEC lysate digest (~25 μg each) were used for PRISM-SRM and IMAC-SRM measurements, respectively.

isoforms combined since all heavy internal standards were spiked with the same concentrations.

At 10 min time point, a significant increase in levels of both dual-phosphorylated pTpY-ERK2 and monophosphorylated pY-ERK2 was observed for all EGF doses (Figure 3A). At 0.1 ng/mL of EGF, nearly half of ERK2 was phosphorylated (pTpY-ERK2, 30.5%; pY-ERK2, 15.6%) and at 0.3 ng/mL the ERK2 activation was close to maximal (pTpY-ERK2, 37.8%; pY-ERK2, 15.6%). Monophosphorylated pT-ERK2 remained at a very low level, although confidently quantified, and its level was essentially unchanged regardless of EGF doses (generally less than 5% of pTpY-ERK2) (Supporting Information Table S2), which is consistent with previous observations.[24,27] Similar dose–response patterns of ERK1 activation were also observed (Supporting Information Figure S4). Overall, our data clearly indicate that both ERK1 and 2 are maximally activated at a very low concentration (~0.3 ng/mL or 0.05 nM) of EGF based on the responses of pTpY-isoform. Interestingly, this concentration of EGF is matched well with the physiological steady state plasma concentrations of EGF in humans, which were reported in the 0.05–0.2 nM range.[34]

At the steady state 2 h EGF stimulation, the levels of ERK phosphorylation in HMEC were significantly reduced compared to those observed at 10 min but show similar dose–response patterns for each isoforms (Figure 3B). The dose response curve did not saturate until 3.0 ng/mL EGF, in contrast to saturation at 0.3 ng/mL at the 10 min time point (Figures 3A and B).

Next, we attempted to examine the relationship between the EGF receptor occupancy and ERK responses. Binding of EGF to its receptor is known to change over time due to its consumption by cells and receptor down-regulation.[35,36] To correct for these effects, we calculated the number of occupied EGFR at each dose of EGF at both 10 min and 2 h as we have previously described,[35] and verified these calculations by comparing them to radio-labeled EGF binding using the same cell type (Supporting Information Figure S6). When we compared the relationship

DOI: 10.1021/ac503797x
Anal. Chem. 2015, 87, 1103–1110

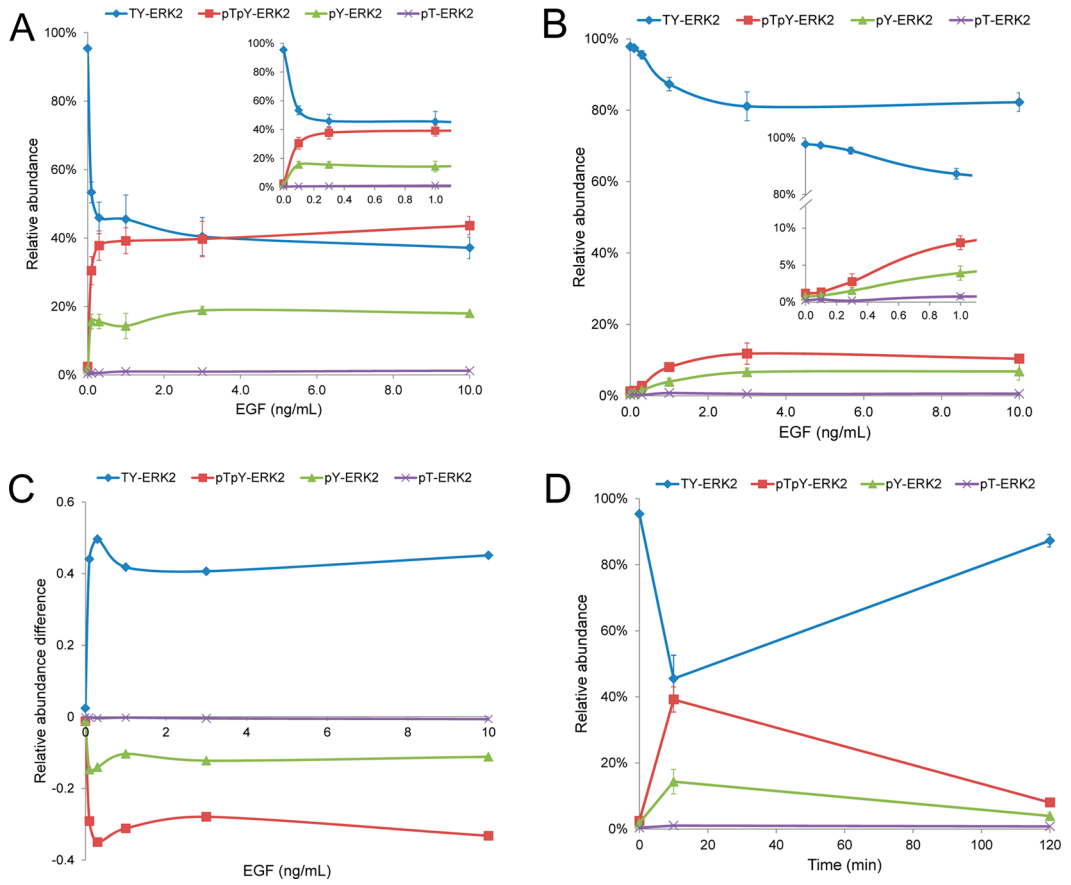

Figure 3. Quantification of ERK phosphorylation dynamics in the HMEC treated with different EGF concentrations (0, 0.1, 0.3, 1.0, 3.0, 10.0 ng/mL). (A) Dose response curves at 10 min stimulation with SD (n = 3). (B) Dose response curves at 2-h stimulation with SD (n = 3). (C) Relative changes in the ERK2 phosphorylation stoichiometries between 10 min stimulation and 2-h stimulation (Supporting Information Table S4). (D) Time-dependent ERK2 phosphorylation changes after 1 ng/mL EGF stimulation with SD (n = 3).

between EGFR occupancy and ERK phosphorylation, we found that at 10 min it was half-maximal when only ~250 EGFR per cell were occupied and maximal at ~1200 EGFR per cell. At the maximal point, we observed ~7.9×10^4 molecules of pTpY-ERK per cell (Supporting Information Figure S7). By 2 h, however, half-maximal ERK phosphorylation required ~2500 EGFR per cell, a 10-fold increase, and the maximal level of pTpY-ERK per cell was reduced to ~2.3×10^4 molecules, a ~3.5-fold decrease (Supporting Information Table S5). Thus, not only does the sensitivity of the cells to occupied EGFR decrease over time, but the absolute magnitude of ERK phosphorylation decreases as well, indicating the presence of at least two negative feedback mechanisms in the ERK activation pathway.

We also noted that upon EGF treatment, ERK1 activation displayed similar dose−response patterns as ERK2. The measured pTpY form of ERK1 seems to have a much lower stoichiometry compared to the pTpY form of ERK2 (Supporting Information Figure S4). One potential limitation of ERK1-pTpY quantification was that the endogenous peptide and its internal standard do not coelute exactly (Supporting Information Figure S3) because of a possible different conformation of the synthetic phosphopeptide standard, which reduced the accuracy of quantification for ERK1-pTpY.

DISCUSSION

We demonstrate that PRISM-SRM enables the detection and quantification of protein phosphorylation in ERK, a well-studied signal transduction model system. Direct PRISM-SRM was applied to measure the signaling dynamics of ERK phosphorylation in EGF-stimulated HMEC cells. Compared to IMAC, PRISM offers the advantage of unbiased enrichment of all types of phosphopeptides with high recovery using the high-resolution reversed-phase LC separations.[15] However, one of the drawbacks of PRISM-SRM is the limited loading capacity of the overall workflow in that only less than 100 μg of starting materials can be used without significantly reducing the separation efficiency of the capillary LC in PRISM. In contrast, IMAC has almost unlimited sample loading capability for enrichment. Therefore, at higher sample loading conditions IMAC-SRM has the potential to provide the same or even higher levels of sensitivity than PRISM-SRM. Nevertheless, IMAC can also be coupled with PRISM workflow to achieve a higher level of sensitivity for phosphopeptide quantification.

Another challenge in studying phosphorylation is the need to quantify its site-specific stoichiometry. Conventional antibody-based approaches, such as Western blotting, are generally limited to relative quantification without knowing the precise occupancy or stoichiometry. Moreover, site-specific antibodies for phosphorylation sites are generally not available due to the inherent challenge in generating antibodies with high specificity that selectively bind to individual sites.[4] The recently developed nanofluidic proteomic immunoassay (NIA) approach, which incorporates charge-based separation with antibody detection, appears to provide reliable, highly sensitive quantification of phosphorylation isoforms.[22,37] However, the charge-based

DOI: 10.1021/ac503797x
Anal. Chem. 2015, 87, 1103−1110

separation provides limited peak capacity and the NIA approach often cannot provide full baseline separation of individual phosphorylation forms. Compared to these antibody-based approaches, PRISM-SRM provides high specificity for achieving baseline separation of different phosphorylation isoforms, mostly because of the high-resolution LC separation[15,16] and two layers of mass selection for reducing coeluting interferences.[5,6] Therefore, PRISM-SRM should be particularly useful for accurate quantification of individual protein phosphorylation isoforms and determination of their stoichiometries in dynamic signaling networks. Our work also presents a proof-of-principle for PTM quantification using PRISM-SRM. Conceptually, this technique should allow simultaneous quantification without affinity enrichment for multiple stable PTMs in a given pathway to allow the study of PTM crosstalk. Following PRISM fractionation, different types of PTMs can be simultaneously measured by LC-SRM without the need for additional enrichments, thus reducing potential bias. In principle PRISM-SRM is able to perform multiplexed quantification of many PTM sites (e.g., up to 100 sites) similarly as regularly LC-SRM; however, the increased number of target peptides will result in some trade-off in sample throughput due to the need to analyze many fractions per sample.

The assay sensitivity in the dose−response experiments accurately reflected the dose−response patterns for all four isoforms from both ERK1 and ERK2 across multiple biological replicates under both basal and stimulated conditions. We note that most previous studies of ERK activations in isolated cells use a much higher EGF concentrations, typically ranging from 10 to 100 ng/mL EGF.[20,38] While there have been some reports on ERK activation by low doses (0.1 to 1 ng/mL) of EGF,[39,40] the exact dose−response patterns and dose needed to reach maximal activation are still unclear, presumably because of the limitations of Western blot quantification. To the best of our knowledge our work is the first to accurately quantify the dose response patterns for each of the phosphorylated ERK isoforms as a function of dose. Our data suggests that ERK activation is maximal for both pTpY and pY isoforms in HMEC at 0.3 ng/mL at 10 min and 3 ng/mL at 2 h, a range of concentrations much closer to physiological levels.[34]

The dose−response information on ERK isoforms also provides useful data for testing mechanistic models of signaling pathways. For example, there are two proposed models for the activation of ERK by the MEK kinase: distributive versus processive mechanisms.[24,27,30] In the distributive mechanism, active MEK binds to ERK, phosphorylates one residue, and subsequently dissociates producing the monophosphorylated ERK form. The monophosphorylated product then associates with a second molecule of MEK, which then phosphorylates the other residue. Alternatively, in the processive mechanism a single molecule of MEK binds to ERK and phosphorylates tyrosine to form pY-ERK, but the activated MEK does not dissociate from pY-ERK, but processively phosphorylates threonine of pY-ERK to form pTpY-ERK.[27] In silico simulations of the two different ERK phosphorylation mechanisms predict that in the distributive phosphorylation model, the monophosphorylated form of pY-ERK should immediately increase following EGF stimulation, followed by a gradual increase in the dual-phosphorylated form of pTpY-ERK.[24,27] In the processive phosphorylation model, the amount of the monophosphorylated pY-ERK should increase in parallel with the amount of the dual-phosphorylated pTpY-ERK with respect to both time and dose.[27] The quantitative dose−response data in our HMEC experiments clearly demonstrated that the increase in the monophosphorylated pY-ERK did not precede, but rather paralleled, the increase in the dual-phosphorylated pYpT-ERK at both the 10 min and 2 h time points (Figure 3 and Supporting Information Figure S4). Furthermore, pY-ERK increased in a dose-dependent manner but did not increase in a bell-shaped manner predicted by the distributive model.[27,29] Additionally, the time course analysis also revealed that the activation pattern of pY-ERK is similar to that of pYpT-ERK but often with lower stoichiometry compared to that of pTpY-ERK (Figure 3D and Supporting Information Figure S5). Taken together, our data support that ERK is phosphorylated in a processive manner, consistent with a recent study of in vivo ERK phosphorylation in HeLa cells.[27,29]

The quantitative data derived from PRISM-SRM also provided useful insight into feedback regulation of the ERK pathway by allowing us to estimate its degree of amplification. By converting EGF concentrations into the level of occupied receptors, we found that at early time point and low levels of EGFR activation, less than 400 occupied EGFR gave rise to more than 60 000 doubly phosphorylated ERK molecules, an amplification of ~150 fold. By 2 h, the amplification had fallen to approximately 5-fold, demonstrating the presence of strong negative feedback. However, we also found that the extent to which the EGFR could activate the ERK pathway was limited. Maximal activation of the ERK pathway was achieved when only around 1000 EGFR were occupied at 10 min, but almost 9000 EGFR were required at 2 h (Supporting Information Table S5). The maximal level of ERK activation also decreased approximately 4-fold at 2 h. Because high levels of receptor occupancy at 2 h did not result in an increase in the level of ERK activation (Supporting Information Table S5), a component downstream of the EGFR, but upstream of ERK, (e.g., adaptor proteins), is likely limiting. It has been reported that activated ERK phosphorylates the adaptor protein SOS1,[41] and the EGFR itself on residue Thr^{669}.[42] The former results in a loss of SOS1 binding to the EGFR[43] and the latter a reduction in the affinity of the EGFR for specific downstream substrates.[44] These two ERK-mediated phosphorylation events could explain the reduction in the maximal extent of ERK phosphorylation and the higher extent of EGFR occupancy needed, respectively. Further experiments will be needed to confirm this hypothesis.

CONCLUSION

The high sensitivity of PRISM-SRM enables accurate quantification of protein phosphorylation dynamics and stoichiometry of ERK isoforms in HMEC starting with only ~25 μg whole cell digest. Compared to IMAC, PRISM enrichment provides >10-fold improvement in sensitivity, attributed largely to higher peptide recovery in the PRISM workflow. The accurate quantification of dose−response of each ERK isoforms confirms that ERK reaches its maximal activation at physiological levels of EGF. The sensitivity of PRISM-SRM potentially enables simultaneous quantification of proteins and their different types of PTMs in a single sample rather than conventional one-by-one quantification of each PTM after serial or parallel enrichment. The resulting quantitative data on individual phosphorylation sites has the potential to elucidate molecular mechanisms of protein kinase activity and signal transduction, thus contributing to improved computational models of multiple phosphorylation events in the regulation of signal transduction.

DOI: 10.1021/ac503797x
Anal. Chem. 2015, 87, 1103−1110

■ ASSOCIATED CONTENT

Supporting Information

Supplemental tables and figures This material is available free of charge via the Internet at http://pubs.acs.org.

■ AUTHOR INFORMATION

Corresponding Authors

*E-mail: steven.wiley@pnnl.gov.
*E-mail: weijun.qian@pnnl.gov.

Notes

The authors declare no competing financial interest.

■ ACKNOWLEDGMENTS

Portions of the research were supported by NIH Grants DP2OD006668, P41GM103493, and U24-CA-16001901. The experimental work described herein was performed in the Environmental Molecular Sciences Laboratory, Pacific Northwest National Laboratory, a national scientific user facility sponsored by the DOE under Contract DE-AC05-76RL0 1830.

■ REFERENCES

(1) Ullrich, A.; Schlessinger, J. *Cell* **1990**, *61*, 203−12.
(2) Ficarro, S. B.; McCleland, M. L.; Stukenberg, P. T.; Burke, D. J.; Ross, M. M.; Shabanowitz, J.; Hunt, D. F.; White, F. M. *Nat. Biotechnol.* **2002**, *20*, 301−5.
(3) Wolf-Yadlin, A.; Hautaniemi, S.; Lauffenburger, D. A.; White, F. M. *Proc. Natl. Acad. Sci. U. S. A.* **2007**, *104*, 5860−5.
(4) O'Neill, R. A.; Bhamidipati, A.; Bi, X.; Deb-Basu, D.; Cahill, L.; Ferrante, J.; Gentalen, E.; Glazer, M.; Gossett, J.; Hacker, K.; Kirby, C.; Knittle, J.; Loder, R.; Mastroieni, C.; Maclaren, M.; Mills, T.; Nguyen, U.; Parker, N.; Rice, A.; Roach, D.; Suich, D.; Voehringer, D.; Voss, K.; Yang, J.; Yang, T.; Vander Horn, P. B. *Proc. Natl. Acad. Sci. U. S. A.* **2006**, *103*, 16153−8.
(5) Shi, T.; Su, D.; Liu, T.; Tang, K.; Camp, D. G., 2nd; Qian, W. J.; Smith, R. D. *Proteomics* **2012**, *12*, 1074−92.
(6) Lange, V.; Picotti, P.; Domon, B.; Aebersold, R. *Mol. Syst. Biol.* **2008**, *4*, 222.
(7) Bisson, N.; James, D. A.; Ivosev, G.; Tate, S. A.; Bonner, R.; Taylor, L.; Pawson, T. *Nat. Biotechnol.* **2011**, *29*, 653−8.
(8) Zheng, Y.; Zhang, C.; Croucher, D. R.; Soliman, M. A.; St-Denis, N.; Pasculescu, A.; Taylor, L.; Tate, S. A.; Hardy, W. R.; Colwill, K.; Dai, A. Y.; Bagshaw, R.; Dennis, J. W.; Gingras, A. C.; Daly, R. J.; Pawson, T. *Nature* **2013**, *499*, 166−71.
(9) Ndassa, Y. M.; Orsi, C.; Marto, J. A.; Chen, S.; Ross, M. M. *J. Proteome Res.* **2006**, *5*, 2789−99.
(10) Bodenmiller, B.; Mueller, L. N.; Mueller, M.; Domon, B.; Aebersold, R. *Nat. Methods* **2007**, *4*, 231−7.
(11) Thingholm, T. E.; Jensen, O. N.; Robinson, P. J.; Larsen, M. R. *Mol. Cell Proteomics* **2008**, *7*, 661−71.
(12) Villen, J.; Gygi, S. P. *Nat. Protoc* **2008**, *3*, 1630−8.
(13) Kruger, M.; Kratchmarova, I.; Blagoev, B.; Tseng, Y. H.; Kahn, C. R.; Mann, M. *Proc. Natl. Acad. Sci. U. S. A.* **2008**, *105*, 2451−6.
(14) Fila, J.; Honys, D. *Amino Acids* **2012**, *43*, 1025−47.
(15) Shi, T.; Fillmore, T. L.; Sun, X.; Zhao, R.; Schepmoes, A. A.; Hossain, M.; Xie, F.; Wu, S.; Kim, J. S.; Jones, N.; Moore, R. J.; Pasa-Tolic, L.; Kagan, J.; Rodland, K. D.; Liu, T.; Tang, K.; Camp, D. G., 2nd; Smith, R. D.; Qian, W. J. *Proc. Natl. Acad. Sci. U. S. A.* **2012**, *109*, 15395−400.
(16) Shi, T.; Qian, W. J. *Bioanalysis* **2013**, *5*, 267−9.
(17) Shi, T.; Sun, X.; Gao, Y.; Fillmore, T. L.; Schepmoes, A. A.; Zhao, R.; He, J.; Moore, R. J.; Kagan, J.; Rodland, K. D.; Liu, T.; Liu, A. Y.; Smith, R. D.; Tang, K.; Camp, D. G., 2nd; Qian, W. J. *J. Proteome Res.* **2013**, *12*, 3353−61.
(18) Shi, T.; Gao, Y.; Quek, S. I.; Fillmore, T. L.; Nicora, C. D.; Su, D.; Zhao, R.; Kagan, J.; Srivastava, S.; Rodland, K. D.; Liu, T.; Smith, R. D.; Chan, D. W.; Camp, D. G., 2nd; Liu, A. Y.; Qian, W. J. *J. Proteome Res.* **2013**, *13* (2), 875−82.
(19) Prabakaran, S.; Everley, R. A.; Landrieu, I.; Wieruszeski, J. M.; Lippens, G.; Steen, H.; Gunawardena, J. *Mol. Syst. Biol.* **2011**, *7*, 482.
(20) Hahn, B.; D'Alessandro, L. A.; Depner, S.; Waldow, K.; Boehm, M. E.; Bachmann, J.; Schilling, M.; Klingmuller, U.; Lehmann, W. D. *J. Proteome Res.* **2013**, *12*, 637−46.
(21) Yao, Z.; Dolginov, Y.; Hanoch, T.; Yung, Y.; Ridner, G.; Lando, Z.; Zharhary, D.; Seger, R. *FEBS Lett.* **2000**, *468*, 37−42.
(22) Fan, A. C.; Deb-Basu, D.; Orban, M. W.; Gotlib, J. R.; Natkunam, Y.; O'Neill, R.; Padua, R. A.; Xu, L.; Taketa, D.; Shirer, A. E.; Beer, S.; Yee, A. X.; Voehringer, D. W.; Felsher, D. W. *Nat. Med.* **2009**, *15*, 566−71.
(23) Burack, W. R.; Sturgill, T. W. *Biochemistry* **1997**, *36*, 5929−33.
(24) Ferrell, J. E., Jr.; Bhatt, R. R. *J. Biol. Chem.* **1997**, *272*, 19008−16.
(25) Zhao, Y.; Zhang, Z. Y. *J. Biol. Chem.* **2001**, *276*, 32382−91.
(26) Shankaran, H.; Ippolito, D. L.; Chrisler, W. B.; Resat, H.; Bollinger, N.; Opresko, L. K.; Wiley, H. S. *Mol. Syst. Biol.* **2009**, *5*, 332.
(27) Aoki, K.; Yamada, M.; Kunida, K.; Yasuda, S.; Matsuda, M. *Proc. Natl. Acad. Sci. U. S. A.* **2011**, *108*, 12675−80.
(28) Schilling, M.; Maiwald, T.; Hengl, S.; Winter, D.; Kreutz, C.; Kolch, W.; Lehmann, W. D.; Timmer, J.; Klingmuller, U. *Mol. Syst. Biol.* **2009**, *5*, 334.
(29) Aoki, K.; Takahashi, K.; Kaizu, K.; Matsuda, M. *Sci. Rep.* **2013**, *3*, 1541.
(30) Toni, T.; Ozaki, Y.; Kirk, P.; Kuroda, S.; Stumpf, M. P. *Mol. Biosyst* **2012**, *8*, 1921−9.
(31) Ficarro, S. B.; Adelmant, G.; Tomar, M. N.; Zhang, Y.; Cheng, V. J.; Marto, J. A. *Anal. Chem.* **2009**, *81*, 4566−75.
(32) MacLean, B.; Tomazela, D. M.; Shulman, N.; Chambers, M.; Finney, G. L.; Frewen, B.; Kern, R.; Tabb, D. L.; Liebler, D. C.; MacCoss, M. J. *Bioinformatics* **2010**, *26*, 966−8.
(33) Wang, Z.; Yang, H.; Tachado, S. D.; Capo-Aponte, J. E.; Bildin, V. N.; Koziel, H.; Reinach, P. S. *Invest. Ophthalmol. Visual Sci.* **2006**, *47*, 5267−75.
(34) Lemos-Gonzalez, Y.; Rodriguez-Berrocal, F. J.; Cordero, O. J.; Gomez, C.; Paez de la Cadena, M. *Br. J. Cancer* **2007**, *96*, 1569−78.
(35) Knauer, D. J.; Wiley, H. S.; Cunningham, D. D. *J. Biol. Chem.* **1984**, *259*, 5623−31.
(36) Reddy, C. C.; Niyogi, S. K.; Wells, A.; Wiley, H. S.; Lauffenburger, D. A. *Nat. Biotechnol.* **1996**, *14*, 1696−9.
(37) Iacovides, D. C.; Johnson, A. B.; Wang, N.; Boddapati, S.; Korkola, J.; Gray, J. W. *Mol. Cell Proteomics* **2013**, *12*, 3210−20.
(38) Zhang, Y.; Wolf-Yadlin, A.; Ross, P. L.; Pappin, D. J.; Rush, J.; Lauffenburger, D. A.; White, F. M. *Mol. Cell Proteomics* **2005**, *4*, 1240−50.
(39) Shankaran, H.; Wiley, H. S. *Curr. Opin. Genet. Dev.* **2010**, *20*, 650−655.
(40) Borisov, N.; Aksamitiene, E.; Kiyatkin, A.; Legewie, S.; Berkhout, J.; Maiwald, T.; Kaimachnikov, N. P.; Timmer, J.; Hoek, J. B.; Kholodenko, B. N. *Mol. Syst. Biol.* **2009**, *5*, 256.
(41) Corbalan-Garcia, S.; Yang, S. S.; Degenhardt, K. R.; Bar-Sagi, D. *Mol. Cell. Biol.* **1996**, *16*, 5674−82.
(42) Takishima, K.; Griswold-Prenner, I.; Ingebritsen, T.; Rosner, M. R. *Proc. Natl. Acad. Sci. U. S. A.* **1991**, *88*, 2520−4.
(43) Kamioka, Y.; Yasuda, S.; Fujita, Y.; Aoki, K.; Matsuda, M. *J. Biol. Chem.* **2010**, *285*, 33540−8.
(44) Heisermann, G. J.; Wiley, H. S.; Walsh, B. J.; Ingraham, H. A.; Fiol, C. J.; Gill, G. N. *J. Biol. Chem.* **1990**, *265*, 12820−7.

DOI: 10.1021/ac503797x
Anal. Chem. 2015, 87, 1103−1110